Highly active Ag/C nanoparticles containing ultra-low quantities of sub-surface Pt for the electrooxidation of glycerol in alkaline media

Highly active Ag/C nanoparticles containing ultra-low quantities of sub-surface Pt for the electrooxidation of glycerol in alkaline media

Carlos C. Lima[a], Marta V.F. Rodrigues[a], Antonio F.M. Neto[a], Cinthia R. Zanata[b], Cléo T.G.V.M.T. Pires[a], Luelc S. Costa[a,d], José Solla-Gullón[c], Pablo S. Fernández[a,d,*]

[a] *Institute of Chemistry, States University of Campinas (UNICAMP), Campinas SP, 13083-970, Brazil*
[b] *Institute of Chemistry, Federal University of Mato Grosso do Sul (UFMS), Campo Grande MS, 79074-460, Brazil*
[c] *Institute of Electrochemistry, University of Alicante, Apdo. 99, E-03080 Alicante, Spain*
[d] *Center for Innovation on New Energies (CINE), Campinas SP, 13083-841, Brazil*

Keywords:
Silver nanoparticles
Platinum
Glycerol electrooxidation
Electrolysis
Hydrogen

A B S T R A C T

The practical application of Pt-based technologies depends on the lowering in the costs and one way to face this challenge is by reducing the amount of Pt. Herein, we decorate Ag nanoparticles with ultra-small (0.8 %) quantities of Pt and test them for the electrooxidation of glycerol. We showed that the Pt atoms of our catalyst are one order of magnitude more active (in terms of mass activity) than Pt/C commercial catalyst. By performing *in situ* FTIR measurements, electrolysis experiments and HPLC analysis, we showed that both catalysts form mainly glycerate and lactate, but Pt/C is more prone to poisoning and to form carbonate. We suggest that this different behavior is attributed to the high dispersion of the Pt atoms on Ag nanoparticles. The lower probability of finding neighboring Pt atoms diminishes the formation of multiple bonded intermediates, which are precursors for the formation of carbonate and some poisoning intermediates.

1. Introduction

One of the most studied electrochemical reactions is the oxygen evolution reaction [1] because this is a critical bottleneck for the massive production of hydrogen through electrolysis. In addition, considering that solar energy will likely become an important source of energy for this century [2], the storage of its surplus in the form of hydrogen will create new opportunities for several industries.

In this context, the addition in the anode of electrolyzers of biomass-derived resources can importantly contribute by decreasing the required potential input for the production of hydrogen in the cathode and at the same time by producing added-value chemicals [3]. Thus, the electrooxidation of glycerol (EOG), among other alcohols, have been extensively studied in acid and alkaline media, mainly in noble metals electrodes [4–10]. However, the reaction in alkaline media emerges as a better alternative because the current observed is much higher than in acid media [11]. Online HPLC results showed that the reaction produces mainly glycerate at low potentials and formate, glycolate and CO_3^{-2} at higher potentials [12,13]. We have recently shown that the reaction can be highly improved by modifying Pt electrodes by Bi and Pb adatoms, which act blocking the oxidation pathways that breaks the GlOH CeC bonds, thus inhibiting the formation of CO and probably others poisoning species [13,14].

Suzuki et al. [15] showed that the GEOR on Ag polycrystalline electrodes depends on the HO^- and GlOH concentration and that this metal is much less active than Pt (the reaction occurs at relatively high potentials, > 0.8 V *vs.* RHE). Garcia et al. [16] showed that Ag promote the GEOR when it is alloyed to Pt in alkaline media (1:1 Pt:Ag). Besides, through *in situ* XAFS measurements, they also showed that the alloyed material displays a higher electronic density in its d-band. Authors claimed that this electronic effect is probably contributing to the reduction of the catalyst poisoning. Kim et al. [17] modified Ag nanotubes with Pt (3:1 Ag/Pt) using the galvanic exchange method and obtained similar results to those previously reported by Garcia et al. [16].

Ag has been at least about one order of magnitude cheaper than the other noble metals commonly used as catalysts (Pt, Pd and Au) during the last decades [18]. Thus, by considering the different cost of Ag and Pt and the synergistic effects showed by PtAg alloys in previous publications, we propose the use of Pt decorated (with a small quantity of Pt (0.8 % w/w)) carbon supported Ag NPs as advanced electrocatalyst for the GEOR. By using the galvanic replacement technique we can effectively deposit Pt atoms at the Ag surface thus maximizing the Pt usage [19]. We observe that Pt activates Ag/C for the GEOR and that

* Corresponding author at: Institute of Chemistry, States University of Campinas (UNICAMP), Campinas SP, 13083-970, Brazil.
E-mail address: pablosf@unicamp.br (P.S. Fernández).

this activity enhancement is much more important than that shown in previous publications even using very low Pt quantities. By means of *in situ* FTIR and electrolysis coupled to HPLC analysis, we observe that the highly dispersed Pt atoms favors the pathways without C-C breaking, thus diminishing the formation of poisoning.

2. Experimental

2.1. Nanoparticles synthesis

Nanoparticles (NPs) were synthesized adapting the impregnation method described by Pritchard [20], and followed by the galvanic substitution procedure described by Zhang [21]. For the synthesis of 20 % Ag/C, 1.6 g of carbon Vulcan XC-72 and 0.63 g of $AgNO_3$ (Sigma-Aldrich ≥ 99.0 %) were mixed in an agate mortar in order to get a 20 % (w/w). The impregnated material was heat treated at 300 °C for 3 h in a reducing atmosphere (5% H_2/N_2) inside a tubular oven to reduce the Ag ions and form Ag/C NPs. Then, the Ag/C NPs were dispersed in 50 mL of ultrapure water and 150 μL of a 0.1 M of H_2PtCl_6 solution (Sigma-Aldrich ≥ 99.9 %) was added. Then the beaker with the suspension was placed in an oil bath under agitation at 70 ± 4 °C for 30 min to accelerate the galvanic replacement and obtaining Pt(1%)Ag/C–20 % NPs. The resulting solid was washed three times with deionized water and oven dried under a N_2 atmosphere at 60 °C for 12 h.

2.2. Physical characterization

The structures of the samples were determined with an X-ray diffractometer Shimadzu XRD-7000, with Cu-Kα radiation (λ = 1.5046 Å, 40 kV, 30 mA). The determination of Pt and Ag was made by Inductively Coupled Plasma Optical Emission Spectrometry (ICP-OES) (Thermo Scientific iCAP 6000 Series), performed in axial mode under the following operation condition: RF power 1250 W, nebulizer gas flow 0.4 L min^{-1}, auxiliary gas flow 0.5 L min^{-1}. The detection wavelengths selected for the quantification of Ag and Pt were 328,0 nm and 214,4 nm, respectively. X-ray Photoelectron Spectroscopy (XPS) experiments were performed in a K-Alpha Surface Analysis (Thermo Scientific) equipment with an Al-Kα X-ray source (hv = 1486.6 eV) and a flood gun. The investigated area was an ellipse of approximately 300 μm in diameter and three different areas of each sample were examined. 10 scans were accumulated for carbon and 50 for the metals. The binding energies (BE) of the spectra were corrected with that of adventitious carbon C1s (C–C, C–H) at 284.8 eV.

2.3. Transmission electronic microscopy (TEM)

Structural properties (morphology and size) were analyzed by transmission electron microscopy in low and high resolution (TEM/HR-TEM) using a TEM-FEG (JEM 2100 F) field-emission gun transmission electron microscope at the Electron Microscopy Laboratory (LME) at the Brazilian Nanotechnology National Laboratory (LNNano/CNPEM, Campinas-SP, Brazil). Both TEM and HR-TEM images were analyzed with ImageJ free software. High-angle annular dark field STEM (HAADF-STEM) images and elemental mapping by Energy-dispersive X-ray Spectroscopy (EDS) were acquired on the same equipment. For all the microscopy measurements, the samples were prepared 24 h before the experiment by drying a drop of the dispersion on ultrathin carbon film supported on holey carbon (*Ted Pella*).

2.4. FTIR in situ

FTIR experiments were performed using a Frontier FTIR spectrometer (Perkin-Elmer) equipped with MCT (Mercury-Cadmium-Telluride) detector cooled with liquid nitrogen. A conventional three electrode spectroelectrochemical cell with a CaF_2 planar window attached to its bottom was used [22]. A PalmSens (Model PSTrace 4) potentiostat coupled to a Frontier FTIRS spectrometer (Perkin-Elmer) equipped with a MCT detector was used to these experiments. FTIR spectra were obtained in the wavenumber range between 3000 cm^{-1} and 1000 cm^{-1}. Reflectance spectra were collected in presence of 1 mol L^{-1} glycerol +0.5 mol L^{-1} NaOH, being calculated as the ratio (R/R_0), where R represents a spectrum at a given potential and R_0 refers to the spectrum collected at 0.1 V. Each spectrum of the series consists of a coaddition of 50 interferograms collected with spectral resolution of 8 cm^{-1}. The series were obtained during a slow cyclic voltammetry (performed at 1.0 mV s^{-1}) in which the potential scan was stopped and hold every 50 mV for data acquisition.

2.5. HPLC experiments

Long-term electrolysis was carried out in a two compartments cell, separated by a proton-conductive polymer film (Nafion™ membrane) to prevent the passage of products formed in the compartment that contains the working (and reference) electrode and the counter electrode. Electrolysis samples were collected every 30 min for 3 h and analyzed by high-performance liquid chromatography (HPLC). The analysis was performed in a Shimadzu LC-6AD chromatograph with a quaternary pump, a thermostatic column compartment CTO-20A, an UV − vis (SPD-20AV at 205 and 254 nm), and a refractory index (RID-20A) detectors, both kept at 40 °C. Three columns (one Aminex HPX87-H and two Shodex Sugar SH1011) were used with a Bio-Rad 1250131 pre-column, kept at 84 °C. The mobile phase was 0.50 mM H_2SO_4 with a flow rate of 0.6 mL min^{-1}, and the injection volume was 20 μL. To identify and quantify the obtained products, we prepared solutions of several standards (sodium mesoxalete, oxalic acid, tartronic acid, hydroxypyruvic acid, glyoxylic acid, glyceric acid, glycolic acid, glyceraldehyde, lactic acid, formic acid and di-hydroxyacetone). Products concentrations were determined by linear correlation with peaks areas from the standards and the samples. 375 μL of electrolyte samples were collected for HPLC analysis. 125 μL of 2.0 mol.L^{-1} H_2SO_4 were added to each sample to adjust the pH to 2. This was done because some products usually formed are not stable in alkaline medium such as dihydroxyacetone and glyceraldehyde.

3. Results and discussion

3.1. Characterization

Fig. 1 shows the diffractograms of Ag/C and Pt(1%)Ag/C NPs. Ag NPs in Ag/C are in their metallic form and displays a fcc structure. Results for Pt(1%)Ag/C NPs show the presence of metallic Ag NPs

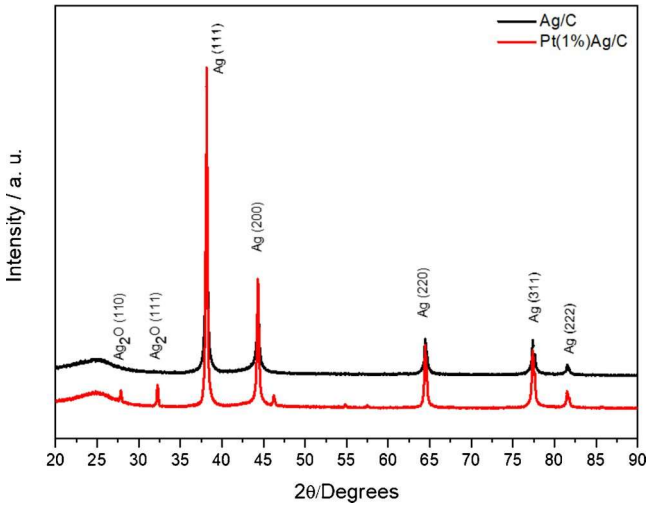

Fig. 1. X-ray Diffraction of Ag/C – 20 % and Pt(1%)Ag/C – 20 % catalysts.

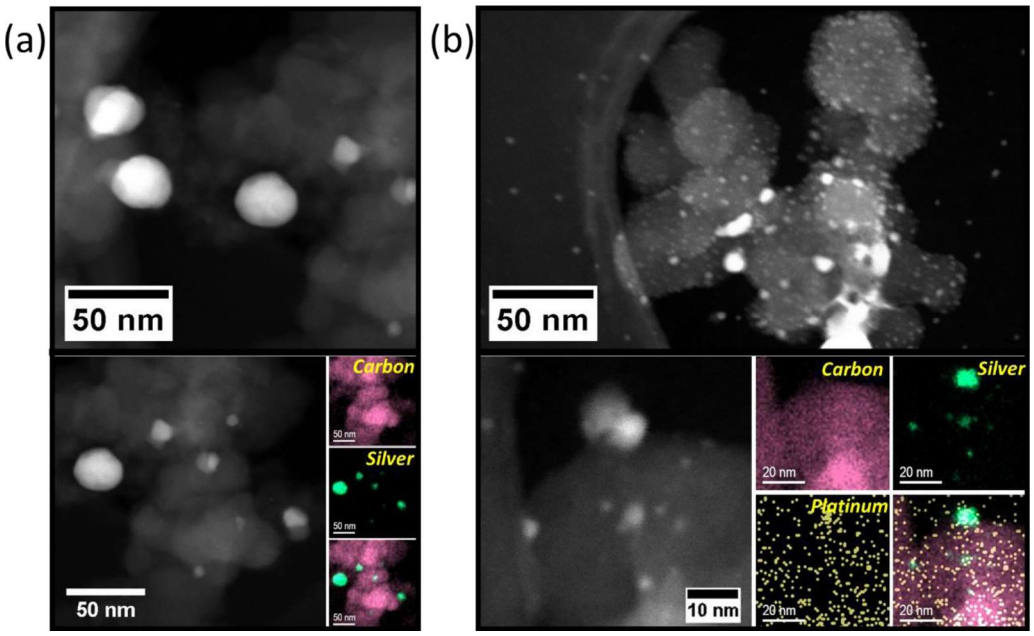

Fig. 2. STEM images and EDS elemental mapping: (a) Ag/C and (b) Pt(1%)Ag/C. Image in a STEM mode (below) with a HAADF detector showing the individual signal of Ag, C and Pt.

(JCPDS No. 04-0783), but also the presence of Ag_2O (JCPDS No. 41-1104), which was formed due to the oxidation promoted by Pt ion [23,24].

A Pt/Ag ratio of 0.74 % in weight was determined by ICP (see supporting info for details). The very low concentration of the well-spread Pt atoms (see below) make impossible to observe the characteristic Pt XRD features.

Fig. 2 shows some representative TEM images of Ag/C and Pt (1%)Ag/C NPs. Ag/C image shows that the catalyst is formed by Ag NPs with a particle diameter smaller than 50 nm, however, there are regions that contain larger particles. Fig. 2b shows that the contact with Pt ions induce the formation of small Ag NPs homogeneously distributed on the catalyst with some small regions with larger particles of Ag. To monitor the presence of Pt in the modified Ag NPs we took images in the STEM mode using a HAADF detector (Fig. 2b). The EDS mapping of the Fig. 2b shows the presence of Ag, carbon and Pt signal coming from all the sample but with more intensity (more spots) right in the regions where the Ag signal is higher, suggesting the deposition of Pt over the Ag NPs as expected when using the galvanic replacement method. However, it is important to emphasize that, the accumulated Pt signal is low. Thus, we confirm the presence of Pt, performing the compositional mapping in regions of the sample where there is particle agglomeration (figure S1), increasing the acquisition time. Thus, it was possible to prove the presence of Pt in regions with a high concentration of Ag NPs.

Fig. 3 shows XPS spectra for Ag and Pt for Pt(1%)Ag/C confirming again the presence of Pt. The Pt/Ag ratio determined by XPS was ~7 % (for details see the supporting information), *i.e.*, an order of magnitude higher than the value obtained through ICP indicating that most of the Pt atoms are at the outer part of the catalyst. The $Pt4f_{7/2}$ peak can be fitted with two gaussian curves, centered at 71.0 eV and 72.7 eV, corresponding to the binding energies of Pt^0 and PtO, respectively (Fig. 3 and table SX) [25]. The XPS peaks for Ag can be fitted with just one gaussian and the binding energy agrees with the predominance of metallic Ag [25], in accordance with the DRX results. The relatively high size of the Ag NPs makes a low fraction of the Ag atoms to be on the surface of the nanoparticle and these are the atoms that easily form oxides when exposed to the atmosphere. In fact, this oxidation of the atoms at the outermost layer explains the presence of two Pt species. However, a careful analysis of the presence of the metallic oxides would in principle not to contribute extensively to the discussion of the electrochemical behavior of the material as the oxidation state of these atoms is electrochemically controlled during the experiment.

Fig. 4 shows the electrochemical characterization of Ag/C and Pt (1%)Ag/C. Fig. 4a and c shows that when both catalysts are cycled in potentials below the Ag oxide formation (> 1.1 V) they behave in a similar way, *i.e.*, at potentials higher than 0.0 V a capacitor like behavior is observed and when we move towards lower potentials a negative current arises due to the hydrogen evolution reaction (HER). If the catalysts are cycled until the oxide formation region (Fig. 4b and d), we observed, in both samples, the characteristic features associated with the Ag oxidation-reduction. However, interestingly, a clear activation (the potential shift to positive values) of the HER is observed for increasing upper potential values. In addition, a clear and wide oxidation contribution at 0.5 V attributed to the oxidation of hydrogen (previously formed in the negative scan) is observed for the Pt containing catalyst (Fig. 4b). These features suggest a segregation of Pt atoms from the core or sub-surface of the Ag NPs to the surface. A similar behavior was found by Solla-Gullon et al. for Pt deposited on gold [24]. For sake of comparison, the same experiment is performed for Ag/C (Fig. 4d), and the results show a stable voltammogram independently of the upper potential limit.

To end with this section, we will summarize the most important results of the characterizations. XRD showed that the addition of Pt ions to the Ag/C dispersion partially oxidizes the Ag NPs to Ag_2O. ICP, XPS, TEM and cyclic voltammetry confirm the presence of Pt in Pt(1%)Ag/C. The Ag/Pt ratio determined by ICP was 0.8 % w/w, *i.e.*, close to the nominal (1% w/w), a much lower value than that determined by XPS (~7%). The XPS results indicate that the Pt atoms are mainly at the surface of the catalyst and some of them in the outermost layer forming oxides. TEM images showed that Pt(1%)Ag/C have Ag NPs with a wide size distribution and, when coupled to EDS, that the Pt atoms are mainly deposited on the surface of the Ag NPs. Very interestingly, CV experiments shows that most of the Pt atoms are not in contact with the electrolyte, but if the electrode is cycled up to the region of the Ag oxide formation-reduction we observe features for Pt (higher hydrogen evolution, hydrogen oxidation and we will also show a remarkable activity improvement of the EOG). This experiment suggest that even if most of the Pt atoms are at the surface (were detected by XPS) an important

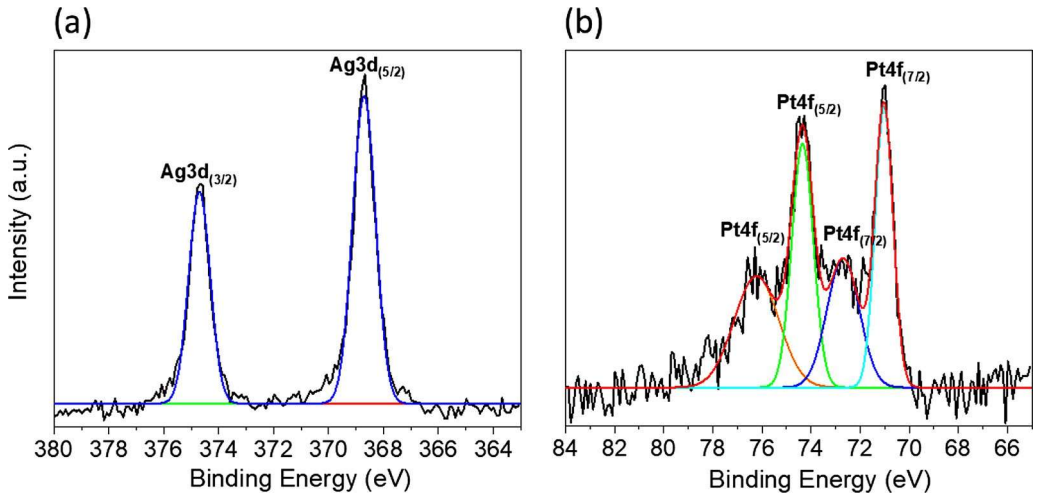

Fig. 3. XPS spectra of the Pt(1%)Ag/C catalyst, showing the high resolution in binding energy ranges of the Ag 3d and Pt 4f signals.

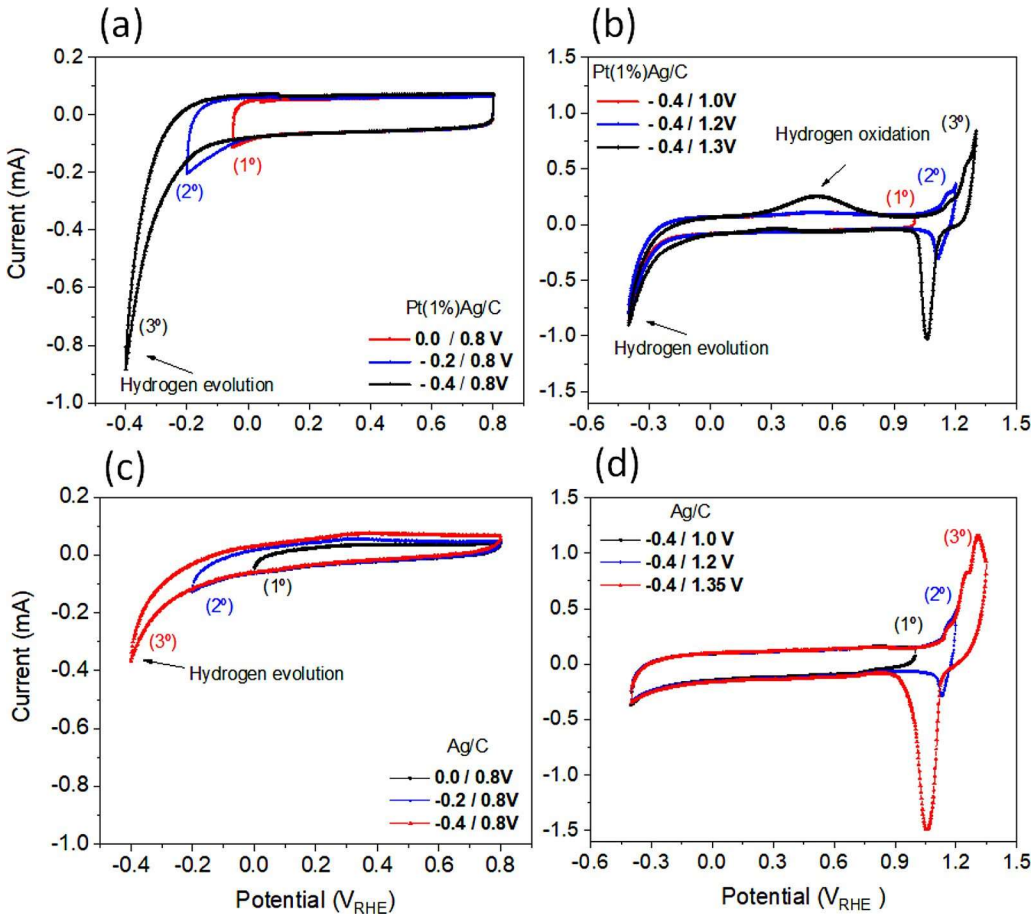

Fig. 4. Cyclic voltammograms performed in NaOH 0.5 mol.L^{-1} for: (a) Pt (1%)Ag/C in the electric double layer region and hydrogen evolution. (b) Pt (1%)Ag/C in the electric double layer region, hydrogen evolution and entering in the Ag oxide formation region. This protocol induces changes in the electrode surface promoting the generation and oxidation of hydrogen. (c) Ag/C in the electric double layer region and hydrogen evolution. (d) Ag/C in the electric double layer region, hydrogen evolution and entering in the Ag oxide formation region. scan rate: 50 mV.s^{-1}.

fraction of the atoms are located at the sub-surface of the Ag NPs, *i.e.*, they are not exactly in the NPs surface (outermost layer) but in the layers bellow where they are not electrochemically active. However, they should be close enough to the surface as to give XPS signals and to easily reach the surface when it is subjected to an electrochemical roughening procedure. This last conclusion is also supported for computational experiments. Hu et al., showed that Ag-Pt NPs tend to have Ag enriched surface and that if the Ag:Pt ratio is high enough, as it is in our case, the NPs form onion-like structure with Ag atoms at the surface, Pt atoms at the sub-surface and Ag at the core [26].

3.2. Electrochemical oxidation of glycerol

Fig. 5a reports the EOG with the Pt(1%)Ag/C electrocatalysts, before and after the electrochemical activation of the material. The activation gives rise to an evident improvement in activity and the peak current density increases about three times in comparison with the non-activated sample. This clear activation again points out the segregation of Pt from the inner parts of the sample to the surface. Also, for the sake of comparison, Fig. 5b also includes the response of a Pt/C 20 % ETEK (the benchmarking commercial catalyst widely used in the field of fuel cell research and that we will call Pt/C from now on). The results

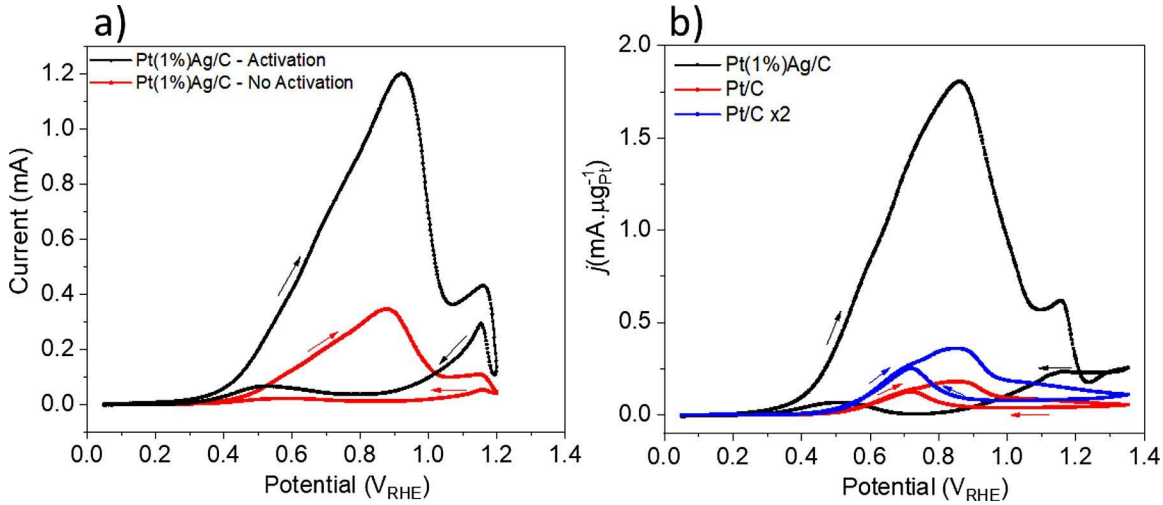

Fig. 5. Cyclic voltammograms obtained in 0.5 mol.L^{-1} NaOH and 1.0 M GlOH solution at scan rate 10 mVs^{-1}. (a) For Pt(1%)Ag/C (before and after the activation) and (b) for Pt(1%)Ag/C-Activated (black line) and Pt/C (red line). We also add the response of Pt/C (blue line) where the currents were multiplied by a factor of 2, to show the activity of this materials if the currents are normalized just by considering the Pt atoms at the surface of the NPs. This result confirms that the activity improvement can not only be justified by a better Pt utilization (For interpretation of the references to colour in this figure legend, the reader is referred to the web version of this article).

obtained clearly shows the excellent properties of the Pt(1%)Ag/C electrocatalysts in terms of mass activity. It is worth mention that the Pt (1%)Ag/C was pre-conditioned by potential cycling as previously shown in Fig. 4. As previously states, this pretreatment induces the segregation of the Pt atoms to the surface, what consequently improves the activity of the sample for the GEOR. Unfortunately, due to the ultra-low Pt loading, the characteristics features associated to the so-called hydrogen region are missing which does not allow the determination of the electroactive surface area to be properly performed. In any case, the clear enhancement in mass activity points out the superior activity of the modified Ag material. Normalizing the data by the Pt mass is widely used as it is motivated for an economic point of view [27] because Pt is by far a much more expensive material than Ag. To understand if the activity improvement is due to a better Pt utilization or if in fact the activity per Pt atom in Pt(1%)Ag/C is higher, another option to normalize the activity is considering only the Pt atoms at the surface of the catalyst. The commercial catalyst is composed of Pt NPs of about 3–4 nm [28–30], which means that only about half of the Pt atoms are right at the surface of the NPs as shown in Figure S3. Therefore, the current values for Pt/C in Fig. 5 were also multiplied by a factor of two to account this aspect. Even in this situation, and assuming that for the Pt(1%)Ag/C all Pt atoms are at the surface (which is certainly not true), the activity of the Pt(1%)Ag/C sample remains being more than 5 times superior than the commercial electrocatalyst.

To better understand the electrochemical results in terms of the products formed during the electrochemical oxidations, we have performed *in situ* FTIR and long-term electrolysis coupled to HPLC. Our FTIR results (Fig. 6) are rather similar to previously published results obtained with polycrystalline Pt electrodes and carefully discussed elsewhere [13,14]. At 0.50 V and 0.6 V several bands start to develop for both materials, one centered at 1580cm^{-1} likely due to the production of formate and/or glycerate and a very broad band centered at 1400 cm^{-1} due to the generation of CO_3^{-2}. The broad band centered at 1400 cm^{-1} clearly displays three bands mounted to that for CO_3^{-2} centered at 1310, 1350 and 1380 cm^{-1} (Fig. 6a). The bands at 1350 and 1380 cm^{-1} are likely due to the presence of formate and that at 1310 cm^{-1} to oxalate. The most important aspect of these results is the relative intensity of the bands for the carbonyl containing compounds (at 1580 cm^{-1}) and that for CO_3^{-2} (at 1380 cm^{-1}). The intensity ratio 1580 cm^{-1}/1380 cm^{-1} is higher for Pt(1%)Ag/C, indicating that this catalyst likely forms less CO_3^{-2}, relative to the carbonyl containing compounds.

Fig. 7 shows the chromatographs obtained with Pt(1%)Ag/C and Pt/C for different times of electrolysis at 0.8 V. In both cases, the concentration of glycerate and lactate increases linearly with time. While Pt/C produce mainly glycerate, lactate and glycolate, Pt(1%)Ag/C generates glycerate, lactate, glycolate and formate. Oxalate was detected by FTIR but not by HPLC, because it retention time coincides with the H^+ from sulfuric acid at 1.0 min. We have also calculated the faradaic efficiency (FE) for every product detected by HPLC in both catalysts. The total FE is around 60 % and 90 % for Pt/C and Pt(1%)Ag/C respectively, for 30 min of electrolysis (table S1). The results are in line with the FTIR, which suggest a higher production of CO_3^{-2} with Pt/C. As the ion is not detected by the HPLC method, the FE due to the complete oxidation of the glycerol molecule is not counted here. Thus, the higher the CO_3^{-2} production is the lower the sum of the FE.

4. General discussion

In this work we have studied the activity and selectivity of a catalyst containing small quantities of Pt deposited at the subsurface of Ag/C. As previously shown, it is extremely difficult to assert if the Pt atoms are forming clusters, are in the form of isolated atoms or, more probably, dispersed forming several kinds of structures at the subsurface of Ag. However, the combination of several techniques suggest that it is a heterogeneous material where Pt atoms are very dispersed and form some aggregates that permitted us to detect them by TEM. We have also shown that the electrochemical oxidation of Ag induce the Pt segregation to the Pt(1%)Ag/C surface, enhancing the activity of the catalyst for the HER, HOR and EOG. CV measurements showed that the activity per Pt atom is much higher on Pt(1%)Ag/C than on Pt/C, even when we take into account that not all the atoms are at the surface in Pt/C and ignoring the same fact for Pt(1%)Ag/C.

Interestingly, as shown in Figure S4, a similar finding is obtained for the electrooxidation of ethanol with Pt(1%)Ag/C, Ag/C and on Pt/C. The comparison between the results with both molecules suggest that our catalyst is more active than Pt/C, not only for these specific molecules, but also for the oxidation of alcohols and polyols.

To get further insights about the structure of Pt(1%)Ag/C and its electrochemical activity, we performed XAFS *in situ* experiments at 0.2 V with Pt(1%)Ag/C and Pt/C (see supporting information). Details about the experimental set up have been recently published by our

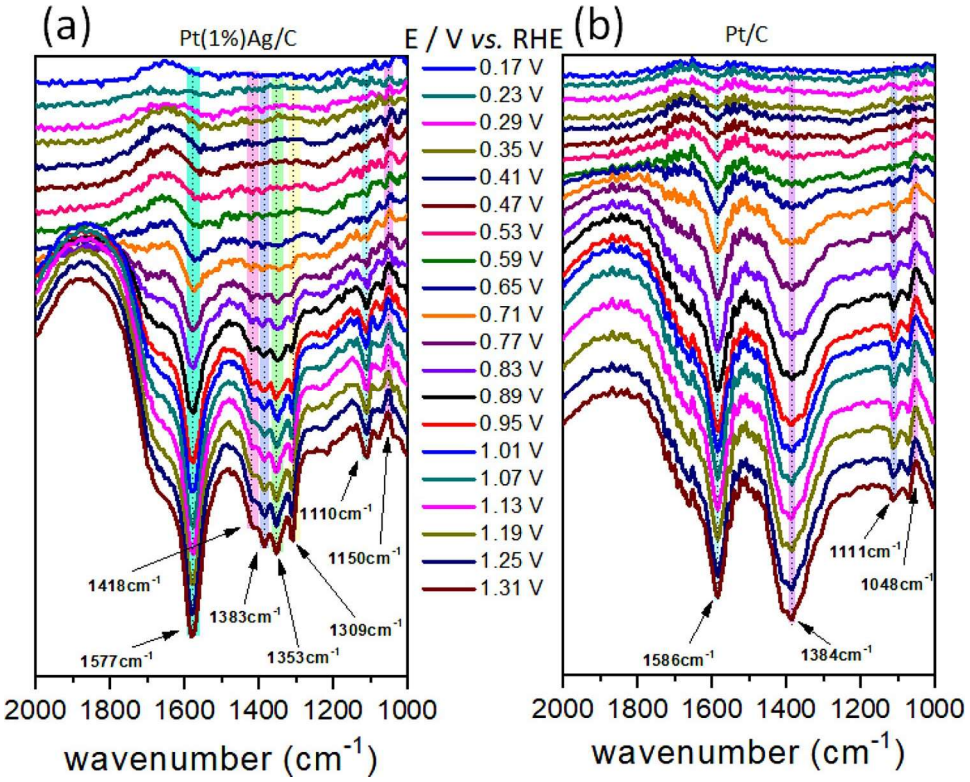

Fig. 6. *In situ* FTIR spectra of: (a) Pt(1%)Ag/C and (b) Pt/C.

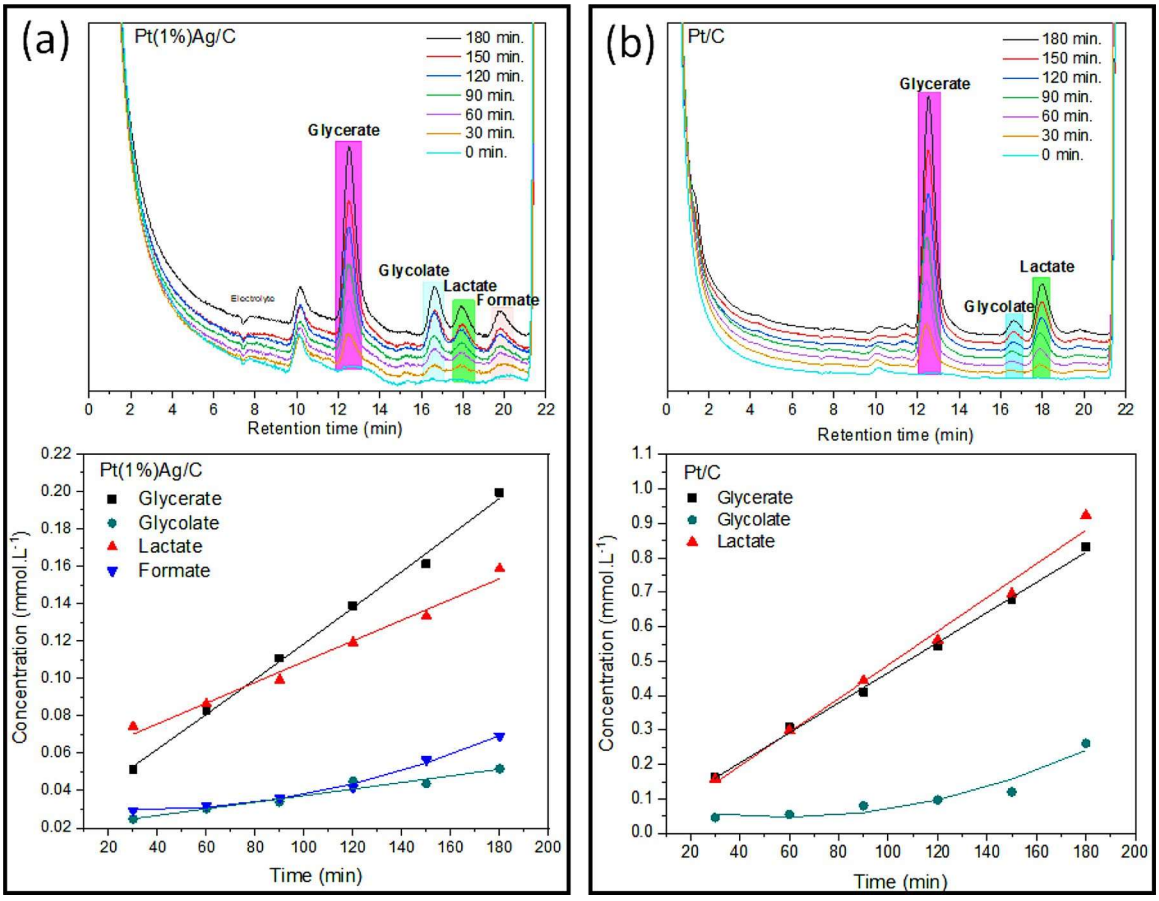

Fig. 7. Chromatograms of the samples obtained at different times during electrolysis at 0.8 V for (a) Pt(1%)Ag/C and (b) Pt/C (above) and the concentration of the main products for each catalyst.

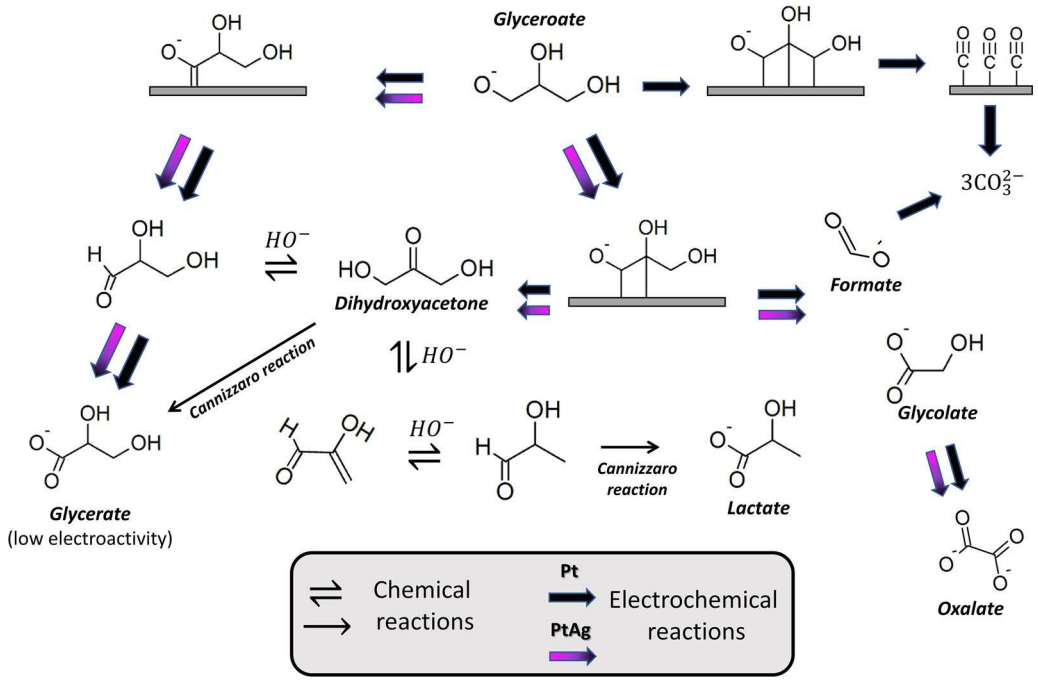

Fig. 8. Proposed reaction pathways for glycerol electrooxidation in alkaline media on Pt(1%)Ag/C and Pt/C based on the products observed using HPLC and FTIR *in situ*. We also add several well-known equilibria for polyols in alkaline media that explain the generation of Lactate.

group [31]. Similar results have been discussed in detail elsewhere [32]. Unfortunately, the results do not show important differences between the catalysts. Again, as Pt(1%)Ag/C is an heterogeneous sample the Pt atoms that are agglomerated have the same contribution to the signal that those well-dispersed, even if most of them are not in contact with the solution and participating of the catalytic process. Besides, this result reinforce that part of the 0.8 % of the Pt atoms of the catalysts Pt (1%)Ag/C are agglomerated, then it is clear that we have underestimated the activity of our catalyst when the currents are normalized by Pt atom at the catalyst surface, making this material even more interesting.

HPLC online and *in situ* FTIR have show that: 1) both catalysts are not selective, 2) Pt/C produce more CO_3^{-2}, *i.e.*, has more ability to break the CeC bonds and 3) Pt(1%)Ag/C forms mainly C_3 products. In some of our previous contributions [13,14], we suggested intermediates and reaction pathways for the electrooxidation of glyceroate (generated by the de-protonation of glycerol in solution) that can be updated and used to explain the findings included in this work (Fig. 8).

As expected, Pt/C show similar results than those reported by some of us for polycrystalline Pt [14,33]. It is interesting to observe that for Pt(1%)Ag/C, the results are similar to those for polycrystalline Pt modified by adatoms. We hypothesized in previous works [13,14] that the presence of the adatoms decreases the probability of finding neighboring Pt atoms, able to generate multiple bonded intermediates, and which are the precursors for C_2 and C_3 product (Fig. 8). Something similar is likely occurring in Pt(1%)Ag/C, where the Pt atoms are highly dispersed and, consequently, the probability of finding neighboring Pt atoms in this catalyst is much lower than in Pt/C, thus justifying the diminution in the production of CO_3^{-2}. This fact can also explain the higher tolerance to poisoning of the Pt(1%)Ag/C, once that multiple bonded intermediate are the precursors of CO and/or other still non-identified poisoning intermediates [34].

Finally, it is worth noting that despite it was possible to observe in the chromatograms peaks due to the formation of Lactate in our previous papers [13,14], we were unable to identify this product [14,33]. Thus, in this work we have updated our mechanism scheme (Fig. 8) including now the production of Lactate. It is important to note that there are several well-known reactions for carbon hydrates in alkaline media, that can be found in any organic chemistry textbooks, and are also present in our system. For example, the Cannizzaro reaction explain the absence of DHA in alkaline media and the formation of Lactate [35,36]. Other well-known equilibria in carbon hydrates chemistry is that between glucose and fructose [37] then we have proposed the equivalent equilibria between glyceraldehyde and DHA. Unfortunately, these reactions are several times not considered in many papers in the field of electrocatalysis, where the authors claim the electrochemical production of substances that several times are formed just by pure chemical steps [38].

5. Conclusions

In this work, we decorated Ag/C NPs with 0.8 % of Pt and obtained a catalyst more than one order of magnitude active than the benchmarking Pt/C. XRD, ICP, XPS, TEM and electrochemical characterization strongly support that the Pt atoms are located at the sub-surface of the Pt(1%)Ag/C and that the electrochemical excursion until the Ag_2O formation induces the Pt atoms segregation activating the material for the HER, HOR and EOG.

In situ FTIR, electrolysis and HPLC analysis showed that Pt(1%)Ag/C and Pt/C form C_3, C_2 and C_1 products. However, Pt/C has more ability to break the CeC bonds, forming more carbonate. This reaction pathway pass through a myriad of intermediates (most of them not known) that act ultimately poisoning the electrode, which explain in part the much higher activity of Pt(1%)Ag/C.

CRediT authorship contribution statement

Carlos C. Lima: Writing - reviewing and editing. Antonio F.M. Neto: Software, Writing - reviewing and editing. Cléo T.G.V.M.T. Pires: Writing - reviewing and editing. Luelc S. Costa: Writing - reviewing and editing. José Solla-Gullón: Conceptualization, Writing - reviewing and editing. Pablo S. Fernández: Supervision, Conceptualization, Writing - reviewing and editing.

Declaration of Competing Interest

The authors declare that there are no conflicts of interest.

Acknowledgements

PSF thanks Fundação de Amparo à Pesquisa do Estado de São Paulo (FAPESP) (grants: 2016/01365-0, 2017/11986-5, 2018/20952-0). CCL thanks Coordenação de Aperfeiçoamento de Pessoal de Nível Superior – Brasil (CAPES) – Finance Code 001. J.S-G. also acknowledges financial support from VITC (Vicerrectorado de Investigación y Transferencia de Conocimiento) of the University of Alicante (UATALENTO16-02). We also thanks Prof. M.A. Zezzi and Luana F. da Costa for the ICP analysis. The authors also extend gratitude to CNPEM open-facilities (LME, and LNNano) and Synchrotron Light Laboratory, CNPEM/MCTIC under proposals 20180571 and 20171115. Finally, we thanks to Dr. Santiago A. Figueroa and Dr. Daniela Zanchet for their assistance with the XAFS experiments and data treatment. We also thanks to Érico and Ângela Teixeira Neto for the assistance in the synthesis and XPS characterization.

Appendix A. Supplementary data

References

[1] Z.W. Seh, J. Kibsgaard, C.F. Dickens, I. Chorkendorff, J.K. Nørskov, T.F. Jaramillo, Combining theory and experiment in electrocatalysis: insights into materials design, Science (80-.) 355 (2017), https://doi.org/10.1126/science.aad4998 eaad4998.

[2] Shell, Shell Scenarios: Sky - Meeting the Goals of the Paris Agreement, (2018), p. 72.

[3] Y. Holade, N. Tuleushova, S. Tingry, K. Servat, T.W. Napporn, H. Guesmi, D. Cornu, K.B. Kokoh, Recent advances in the electrooxidation of biomass-based organic molecules for energy, chemicals and hydrogen production, Catal. Sci. Technol. 10 (2020) 3071–3112, https://doi.org/10.1039/C9CY02446H.

[4] C.A. Angelucci, J. Souza-Garcia, P.S. Fernández, P.V.B. Santiago, R.M.L.M. Sandrini, Glycerol electrooxidation on noble metal electrode surfaces, Encycl. Interfacial Chem. Elsevier, 2018, pp. 643–650, https://doi.org/10.1016/B978-0-12-409547-2.13330-X.

[5] F. Gao, H. Xu, Y. Zhang, J. Wang, C. Wang, Y. Du, Facile construction of pompon-like PtAg alloy catalysts for enhanced ethylene glycol electrooxidation, Int. J. Hydrogen Energy 43 (2018) 9644–9651, https://doi.org/10.1016/j.ijhydene.2018.04.005.

[6] F. Gao, Y. Zhang, P. Song, J. Wang, B. Yan, Q. Sun, L. Li, X. Zhu, Y. Du, Shape-control of one-dimensional PtNi nanostructures as efficient electrocatalysts for alcohol electrooxidation, Nanoscale 11 (2019) 4831–4836, https://doi.org/10.1039/c8nr09892a.

[7] E.A. Monyoncho, T.K. Woo, E.A. Baranova, Ethanol electrooxidation reaction in alkaline media for direct ethanol fuel cells, SPR Electrochem. 15 (2019) 1–57, https://doi.org/10.1039/9781788013895-00001.

[8] T. Wang, F. Li, H. Huang, S. Yin, P. Chen, P. Jin, Y. Chen, Porous Pd-PdO Nanotubes for Methanol Electrooxidation, 2000534 (2020), pp. 1–10, https://doi.org/10.1002/adfm.202000534.

[9] O.A. Petrii, The progress in understanding the mechanisms of methanol and formic acid electrooxidation on platinum group metals (a review), Russ. J. Electrochem. 55 (2019) 3–38, https://doi.org/10.1134/S1023193519010129.

[10] L. Gong, Z. Yang, K. Li, W. Xing, C. Liu, J. Ge, Recent development of methanol electrooxidation catalysts for direct methanol fuel cell, J. Energy Chem. 27 (2018) 1618–1628, https://doi.org/10.1016/j.jechem.2018.01.029.

[11] Y. Kwon, K.J.P. Schouten, M.T.M. Koper, Mechanism of the catalytic oxidation of glycerol on polycrystalline gold and platinum electrodes, ChemCatChem 3 (2011) 1176–1185, https://doi.org/10.1002/cctc.201100023.

[12] A.C. Garcia, Y.Y. Birdja, G. Tremiliosi-Filho, M.T.M. Koper, Glycerol electro-oxidation on bismuth-modified platinum single crystals, J. Catal. 346 (2017) 117–124, https://doi.org/10.1016/j.jcat.2016.12.013.

[13] M.B.C. de Souza, R.A. Vicente, V.Y. Yukuhiro, C.T.G. Vilela Menegaz Teixeira Pires, W. Cheuquepán, J.L. Bott Neto, J. Solla-Gullon, P.S. Fernandez, Bi-modified Pt electrodes towards glycerol electrooxidation in alkaline solution: effects on activity and selectivity, ACS Catal. (2019), https://doi.org/10.1021/acscatal.9b00190 acscatal.9b00190.

[14] M.B.C. de Souza, V.Y. Yukuhiro, R.A. Vicente, C.T.G. Vilela Menegaz Teixeira Pires, J.L. Bott-Neto, P.S. Fernández, Pb- and Bi-modified Pt electrodes toward glycerol electrooxidation in alkaline media. Activity, selectivity, and the importance of the Pt atoms arrangement, ACS Catal. 10 (2020) 2131–2137, https://doi.org/10.1021/acscatal.9b04805.

[15] N.Y. Suzuki, P.V.B. Santiago, T.S. Galhardo, W.A. Carvalho, J. Souza-Garcia, C.A. Angelucci, Insights of glycerol electrooxidation on polycrystalline silver electrode, J. Electroanal. Chem. 780 (2016) 391–395, https://doi.org/10.1016/j.jelechem.2016.02.020.

[16] A.C. Garcia, E.B. Ferreira, V.V. Silva de Barros, J.J. Linares, G. Tremiliosi-Filho, PtAg/MnOx/C as a promising electrocatalyst for glycerol electro-oxidation in alkaline medium, J. Electroanal. Chem. 793 (2017) 188–196, https://doi.org/10.1016/j.jelechem.2016.11.053.

[17] Y. Kim, H. Kim, W. Bae Kim, PtAg Nanotubes for Electrooxidation of Ethylene Glycol and Glycerol in Alkaline Media, (2014), https://doi.org/10.1016/j.elecom.2014.06.007.

[18] Kitco Search, (n.d.). https://www.kitco.com/search/?q=silver (accessed September 30, 2019).

[19] S.T. Hunt, Y. Román, R.- Leshkov, Principles and methods for the rational design of core–Shell nanoparticle catalysts with ultralow noble metal loadings, Acc. Chem. Res. 51 (2018) 25, https://doi.org/10.1021/acs.accounts.7b00510.

[20] J.C. Pritchard, Q. He, E.N. Ntainjua, M. Piccinini, J.K. Edwards, A.A. Herzing, A.F. Carley, J.A. Moulijn, C.J. Kiely, G.J. Hutchings, The effect of catalyst preparation method on the performance of supported Au-Pd catalysts for the direct synthesis of hydrogen peroxide, Green Chem. 12 (2010) 915–921, https://doi.org/10.1039/b924472g.

[21] H. Zhang, T. Watanabe, M. Okumura, M. Haruta, N. Toshima, Crown Jewel catalyst: How neighboring atoms affect the catalytic activity of top Au atoms? J. Catal. 305 (2013) 7–18, https://doi.org/10.1016/j.jcat.2013.04.012.

[22] T. Iwasita, F.C. Nart, In situ infrared spectroscopy at electrochemistry interfaces, Prog. Surf. Sci. 55 (1997) 271–340.

[23] J. Wisniewska, C.M. Yang, M. Ziolek, Changes in bimetallic silver – platinum catalysts during activation and oxidation of methanol and propene, Catal. Today (2019) 89–96, https://doi.org/10.1016/j.cattod.2018.03.001.

[24] J. Solla-Gullón, A. Aldaz, J. Clavilier, Ultra-low platinum coverage at gold electrodes and its effect on the hydrogen reaction in acidic solutions, Electrochim. Acta 87 (2013) 669–675, https://doi.org/10.1016/j.electacta.2012.09.043.

[25] C.J.P. Alexander, V. Naumkin, Anna Kraut-Vass, Stephen W. Gaarenstroom, NIST X-ray photoelectron spectroscopy database, Meas. Serv. Div. Natl. Inst. Stand. Technol. 20899 (2012), https://doi.org/10.18434/T4T88K 20899.

[26] L. Deng, H. Deng, S. Xiao, J. Tang, W. Hu, Morphology, dimension, and composition dependence of thermodynamically preferred atomic arrangements in Ag-Pt nanoalloys, Faraday Discuss. 162 (2013) 293–306, https://doi.org/10.1039/c3fd20138d.

[27] C.R. Zanata, P.S. Fernández, A.B. Santos, G.C. da Silva, G.A. Camara, C.A. Martins, Estimating the time-dependent performance of nanocatalysts in fuel cells based on a cost-normalization approach, J. Braz. Chem. Soc. 27 (2016) 1980–1988, https://doi.org/10.5935/0103-5053.20160088.

[28] M. Shao, A. Peles, K. Shoemaker, Electrocatalysis on platinum nanoparticles: particle size effect on oxygen reduction reaction activity, Nano Lett. 11 (2011) 3714–3719, https://doi.org/10.1021/nl2017459.

[29] B. Garlyyev, K. Kratzl, M. Rück, J. Michalička, J. Fichtner, J.M. Macak, T. Kratky, S. Günther, M. Cokoja, A.S. Bandarenka, A. Gagliardi, R.A. Fischer, Optimizing the size of platinum nanoparticles for enhanced mass activity in the electrochemical oxygen reduction reaction, Angew. Chemie - Int. Ed. 58 (2019) 9596–9600, https://doi.org/10.1002/anie.201904492.

[30] M. Nesselberger, M. Roefzaad, R. Fayçal Hamou, P. Ulrich Biedermann, F.F. Schweinberger, S. Kunz, K. Schloegl, G.K.H. Wiberg, S. Ashton, U. Heiz, K.J.J. Mayrhofer, M. Arenz, The effect of particle proximity on the oxygen reduction rate of size-selected platinum clusters, Nat. Mater. 12 (2013) 919–924, https://doi.org/10.1038/nmat3712.

[31] J.L. Bott-Neto, M.V.F. Rodrigues, M.C. Silva, E. Batista Carneiro Neto, G. Wosiak, J.C. Mauricio, E.C. Pereira, S.J.A. Figueroa, P. Fernández, Versatile Spectroelectrochemical Cell for in Situ Experiments: Development, Applications and Electrochemical Behavior, (2020), https://doi.org/10.26434/CHEMRXIV.12631034.V1.

[32] A.E. Russell, A. Rose, X-ray absorption spectroscopy of low temperature fuel cell catalysts, Chem. Rev. 104 (2004) 4613–4635, https://doi.org/10.1021/cr020708r.

[33] M.B.C. de Souza, R.A. Vicente, V.Y. Yukuhiro, C.T.G.V.M.T. Pires, W. Cheuquepán, J.L. Bott-Neto, J. Solla-Gullón, P.S. Fernández, Bi-modified Pt electrodes toward glycerol electrooxidation in alkaline solution: effects on activity and selectivity, ACS Catal. 9 (2019) 5104–5110, https://doi.org/10.1021/acscatal.9b00190.

[34] G. Soffiati, J.L. Bott-Neto, V.Y. Yukuhiro, C.T.G.V.M.T. Pires, C.C. Lima, C.R. Zanata, Y.Y. Birdja, M.T.M. Koper, M.A. San-Miguel, P.S. Fernández, Electrooxidation of C_4 polyols on platinum single-crystals: a computational and electrochemical study, J. Phys. Chem. C (2020), https://doi.org/10.1021/acs.jpcc.0c05017 acs.jpcc.0c05017.

[35] C.D. Evans, M. Douthwaite, J.H. Carter, S. Pattisson, S.A. Kondrat, D. Bethell, D.W. Knight, S.H. Taylor, G.J. Hutchings, Enhancing the understanding of the glycerol to lactic acid reaction mechanism over AuPt/TiO2 under alkaline conditions, J. Chem. Phys. 152 (2020), https://doi.org/10.1063/1.5128595.

[36] C. Dai, L. Sun, H. Liao, B. Khezri, R.D. Webster, A.C. Fisher, Z.J. Xu, Electrochemical production of lactic acid from glycerol oxidation catalyzed by AuPt nanoparticles, J. Catal. 356 (2017) 14–21, https://doi.org/10.1016/j.jcat.2017.10.010.

[37] M.J. King-Morris, A.S. Serianni, Hydroxide-catalyzed isomerization of d-[1-13C] mannose: Evidence for the involvement of 3,4-enediols, Carbohydr. Res. 154 (1986) 29–36, https://doi.org/10.1016/S0008-6215(00)90019-3.

[38] Y.Y. Birdja, M.T.M. Koper, The importance of cannizzaro-type reactions during electrocatalytic reduction of carbon dioxide, J. Am. Chem. Soc. 139 (2017) 2030–2034, https://doi.org/10.1021/jacs.6b12008.